Methane recovery from gas hydrate-bearing sediments: An experimental study on the gas permeation characteristics under varying pressure

Accepted Manuscript

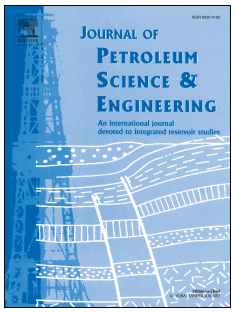

Methane recovery from gas hydrate-bearing sediments: An experimental study on the gas permeation characteristics under varying pressure

Anthony Okwananke, Aliakbar Hassanpouyouzband, Mehrdad Vasheghani Farahani, Jinhai Yang, Bahman Tohidi, Evgeny Chuvilin, Vladimir Istomin, Boris Bukhanov

PII: S0920-4105(19)30514-5

DOI: https://doi.org/10.1016/j.petrol.2019.05.060

Reference: PETROL 6109

To appear in: *Journal of Petroleum Science and Engineering*

Received Date: 21 February 2019

Revised Date: 5 May 2019

Accepted Date: 25 May 2019

Please cite this article as: Okwananke, A., Hassanpouyouzband, A., Vasheghani Farahani, M., Yang, J., Tohidi, B., Chuvilin, E., Istomin, V., Bukhanov, B., Methane recovery from gas hydrate-bearing sediments: An experimental study on the gas permeation characteristics under varying pressure, *Journal of Petroleum Science and Engineering* (2019), doi: https://doi.org/10.1016/j.petrol.2019.05.060.

Methane Recovery from Gas Hydrate-bearing Sediments: An Experimental Study on the Gas Permeation Characteristics under Varying Pressure

Anthony Okwananke[a], Aliakbar Hassanpouyouzband[a], Mehrdad Vasheghani Farahani[a], Jinhai Yang[a,*], Bahman Tohidi[a], Evgeny Chuvilin[b], Vladimir Istomin[b], Boris Bukhanov[b]

[a] Hydrates, Flow Assurance & Phase Equilibria Research Group, Institute of Petroleum Engineering, Heriot-Watt University, Edinburgh EH14 4AS, United Kingdom

[b] Skolkovo Institute of Science and Technology, Moscow 143026, Russia

Abstract

In this paper, characteristics of gas permeation through gas hydrate-bearing sediments were explored under varying differential pressure for three types of sedimentary core samples, including 100 wt. % silica sand, 95 wt. % silica sand + 5 wt. % montmorillonite clay, and consolidated sandstone using a standard core-holder. Results of the experiments indicate that capillary breakthrough, hydrate-forced heave or agglomeration and also Klinkenberg effect play important roles in controlling the gas permeation through different porous sediments, depending on the sediment type and properties such as grain/pore size distribution and degree of consolidation. It was observed that due to the presence of large pores in unconsolidated silica sand core samples, the gas flow is dominated at both hydrate-free and hydrate-bearing cases by the capillary breakthrough mechanism rather than the gas slippage which resulted in direct relationship between the gas permeability and the differential pressure. This mechanism was also observed to be dominant while measuring the gas permeability for the hydrate-free sandstone core sample. For the unconsolidated sand-clay core samples, higher saturation of methane hydrate led to relatively higher gas permeability due to hydrate-forced heave phenomenon which pushed the sediment grains apart from each other or hydrate agglomeration that formed inter-grain pores. Klinkenberg effect became significant for the hydrate-free sand-clay and hydrate-bearing sandstone core samples; however, it was not observed to be dominant in the hydrate-bearing sand-clay core samples due to the hydrate-forced heave and agglomeration until the inlet pressure was sufficiently high.

Keywords*: Methane Recovery; Gas Permeability; Methane Hydrate; Breakthrough Capillary Pressure; Hydrate-forced Heave and Agglomeration; Klinkenberg effect.*

* Corresponding author: petjy@hw.ac.uk

1. Introduction

Gas hydrates are ice-like crystalline compounds composed of cages of water molecules and enclathrated guest molecules (Mehrabian et al., 2018; Sloan Jr, 2003). They form under conditions of high pressure and low temperature. When the guest molecules are a mixture of the components of natural gas such as methane, ethane, propane, carbon dioxide, and nitrogen, they are referred to as natural gas hydrates (Sloan Jr and Koh, 2007). Natural gas hydrates occur in nature under the subsurface of permafrost regions and in the continental margins of world oceans (Collett, 1992; Kvenvolden, 1988; Max and Johnson, 2018). Due to its overwhelming abundance in nature, gas hydrate is regarded as a potential future source of low carbon energy as the global energy system is being decarbonized gradually. This has elicited tremendous research effort towards the development of commercially viable and environmentally safe production techniques (Hassanpouryouzband et al., 2018a). Three major techniques have been proposed, namely, depressurization, thermal stimulation, and chemical inhibitor injection (Holder et al., 1984; Waite et al., 2009). Depressurisation induces hydrate dissociation by reducing the system pressure below the hydrate stability pressure at the prevailing reservoir temperature. Thermal stimulation introduces external heat to shift the system temperature away from equilibrium thus decompose hydrate. The external heat source can be hot water, steam, hot brine or an electromagnetic heat source (Castaldi et al., 2007; Fitzgerald and Castaldi, 2013; Linga et al., 2009a, 2009b; Nakoryakov et al., 2013; Schicks et al., 2013). Injection of chemicals such as glycols and methanol alters the hydrate equilibrium chemically to dissociate hydrate. Combination of any two of the mentioned techniques has also been shown to improve gas recovery efficiency. The most characterised is thermal stimulation combined with depressurisation (Falser et al., 2012; Li et al., 2014; Loh et al., 2014; Sakamoto et al., 2010). CO_2 or CO_2-mixed injection technique can also be utilized for methane recovery based on CO_2-CH_4 exchange (Kang et al., 2014; Masuda et al., 2011; Ohgaki et al., 1996; Schoderbek et al., 2012) and chemical potential shift (Hassanpouryouzband et al., 2018b, 2018a, 2017; Kang et al., 2012; Okwananke et al., 2018) and for geological carbon capture and storage (Hassanpouryouzband et al., 2019a; Yang et al., 2017). Moreover, direct injection of flue gas in permafrost region for CO_2 storage and secondary sealing of CH_4 release into atmosphere through formation of a gas hydrate layer has been proposed (Hassanpouryouzband et al., 2019b). Natural gas hydrate exploitation by CO_2/H_2 injection is also considered as another promising technique, in which the role of H_2 is to decrease the partial pressure of methane and break methane hydrate stability (Sun et al., 2018; Wang et al., 2017).

Apart from flow assurance considerations, particularly avoidance of hydrate reformation in the downhole separation systems (Fu et al., 2019, 2018), the efficiency of gas production from sediments strongly depends on the permeability of hydrate deposits (Waite et al., 2009). The permeability of hydrate-bearing porous media differs markedly from that of non-hydrate-bearing porous media. In general,

permeability of hydrate-bearing sediments is reduced due to the presence of gas hydrate in pores. The permeability change is complicated as it is affected by a number of geological formation factors such as hydrate saturation, porosity, and sediment mineralogy (Moridis et al., 2009; Nimblett and Ruppel, 2003). In particular, the extent of permeability reduction depends on the hydrate formation sites in the porous media. Empirical modelling of permeability showed that, if hydrates form on the surfaces of grains, the reduction in permeability is gradual and minimal, therefore, the effect on fluid flow is also minimal. If hydrates form in the middle of the pores, permeability reduction is pronounced, and even reduces to zero if the pore bodies are completely blocked (Kleinberg et al., 2003). Also, permeability in the presence of hydrate changes as hydrate dissociates. This change impacts directly on pressure communication, fluid flow and ultimately, gas production from hydrate-bearing sediments. Recently, a critical path analysis (CPA) was conducted by Daigle to predict permeability to either water or gas over the entire range of the measured hydrate saturation (Daigle, 2016). It was showed that CPA can appropriately assisted for determination of permeability in hydrate-bearing sediments. However, permeability and relative permeability in gas hydrate-bearing sediments are still peculiar properties which is imperative to be studied.

Permeability measurements using natural core samples in in-situ conditions from hydrate-bearing sediments is often costly and difficult to achieve (Kneafsey et al., 2011; Waite et al., 2009). Pressure coring helps to maintain the samples at near in-situ conditions but does not completely eliminate sample disturbance during coring (Dickens et al., 1995). Also, creep and diffusion processes may cause hydrate re-distribution and change physical properties of the cores when pressure cores are stored for a long time (Waite et al., 2009). Laboratory synthesis of artificial hydrate cores is therefore, a viable alternative for permeability measurements and studies. It has the flexibility of synthesising hydrates with characteristics of interest such as hydrate saturations and preparation processes despite differences in pore-scale growth habits, time scales of hydrate formation, and spatial distribution (Yang et al., 2008). Further discussion in this regard can be found elsewhere (Choi et al., 2014; Long et al., 2009). It should be noted that controlled synthesis of methane hydrate-bearing sediments in laboratory, particularly in a way it forms in nature, has always been a challenge due to low solubility of methane in water (Choi et al., 2014). As a result, hydrate formation from methane gas dissolved in water is a slow process. Hence, more expedient techniques are usually followed in laboratory such as dissolved gas method, partial water saturation method, ice-seeding method, and hydrate premixing method (Waite et al., 2009). Each method could result in different pore-scale habits and different permeation characteristics accordingly (Spangenberg et al., 2005). Nevertheless, the partial water saturation method followed in this work has shown to be fast and reliable enough to make homogeneous synthetic gas hydrate-bearing sediments at desired saturations (Hassanpouryouzband et al., 2019b, 2018a, 2018b, Yang et al., 2019, 2017).

Given the significance of permeability change and the importance of its predictability in the successful exploitation of natural gas hydrate reservoirs, researchers attempted to understand gas permeation mechanisms in hydrate-bearing sediments using different porous media including glass beads, sand, and clay. Kumar et al. experimentally determined gas permeability of packed glass beads with varying saturation of CO_2 hydrate (Kumar et al., 2010). Their results were compared with the theoretical estimates of Kozeny grain models (Kleinberg et al., 2003) for grain coating and pore filling permeability models. They observed that for hydrate saturations less than 35%, the measured permeability values agree better with the grain coating model. On the other hand, for hydrate saturations greater than 35%, the measured permeability values agree better with pore filling models. Kneafsey et al. measured gas permeability with a core holder for dry, moist, frozen, and hydrate-bearing sediments composed of sand and sand/silt mixtures (Kneafsey et al., 2011). They reported that permeability reduced in an order of dry sediments, moist sediments, frozen sediments, and that increase in hydrate saturation resulted in decrease in the permeability of hydrate-bearing sediments. In their water flood experiments, it was observed that water flood was not possible for the sand and sand/silt sediments with the highest hydrate saturation due to extremely low permeability. Delli and Grozic conducted a series of water relative permeability measurements using a triaxial cell (Delli and Grozic, 2014). They formed CO_2 hydrate of saturations up to 45% in Ottawa sand. Their results indicated a gradual reduction in the permeability as hydrate saturation increased, suggesting that hydrate grows in the pore bodies. They developed a hybrid model using a weighted combination of the Kozeny grain-coating and pore-filling models (Scheidegger, 1958). They compared their hybrid model alongside existing theoretical permeability models with the experimental results. Their hybrid model gave closer values to the experimental permeability. Li et al. measured the absolute and water effective permeability of methane hydrate-bearing quartz sand cores with hydrate saturations ranging from 0-31% pore volume at a constant pore pressure of 15 MPa (Li et al., 2017). They used three different grain size ranges of quartz sand of 200-300, 300-450, and 450-600 µm, respectively. Their calculated absolute permeability was significantly higher in the quartz sand with the high grain size. Also, the water effective permeability reduced as the methane hydrate saturation increased. In the hydrate-bearing cores, the measured permeability characteristics for hydrate saturations lower than 10% and higher than 10% differs. Permeability reduction due to increase in hydrate saturation was very significant for the hydrate-bearing sand packs with less than 10% hydrate and became much smaller for those with hydrate saturation above 10%.

Permeability measurement techniques for hydrate bearing sediments have evolved from steady-state gas or water flow to the use of nuclear magnetic resonance (NMR) and X-Ray computed tomography (CT). Kneafsey et al. performed gas permeability measurements on partially saturated sand packs under confining stress using CT scanning (Kneafsey et al., 2011). It was observed gas permeation processes are spatially dependent. They reported decreasing effective permeability as the pore

spaces in the samples became increasingly occupied by gas hydrate. Recently, percolation characteristics of gas hydrate-bearing sediments were comprehensively studied via combining pore network models (PNM) with micro-CT imaging (J.-Q. Wang et al., 2015; J. Wang et al., 2015; Wang et al., 2018, 2016). They extracted the pore network models from the processed 3D micro-CT images taken from laboratory-formed methane hydrate sediments, performed numerical simulations and investigated the effect of hydrate saturation, wettability, interfacial tension, and particle size on the permeability. These studies confirmed that obtaining a realistic structure of hydrate-bearing sediments from micro-CT imaging into pore network model substantially improves the accuracy of the simulations. Chen et al. also used micro-CT for monitoring hydrate growth in a sandpack under the excess gas condition (Chen et al., 2018). They also performed Lattice Boltzmann Method (LBM) for pore-scale determination of gas relative permeability as a function of hydrate saturation. Kleinberg et al. used NMR to study hydrate formation, hydrate growth, and its effect on the relative permeability of water (Kleinberg et al., 2003). They reported that at substantial hydrate saturation, NMR relaxation time measurements showed that hydrate preferentially replaced water in the largest pores rather than coating grain surfaces. The relative permeability to water reduced significantly. The extent of the reduction agreed with hydrate formation in pore bodies rather than on grain surfaces.

A few studies on permeability of hydrate-bearing sediments were reported for clayey sediments. Liu et al. investigated the dependence of gas permeability on methane hydrate-bearing kaolin in the presence of different saturations of hydrate under effective axial stress of 1 MPa and 3 MPa (Liu et al., 2016). Ice-seeding method was used to form hydrate. They observed that with increasing hydrate saturation, gas permeability decreases when the hydrate saturation was less than 4.23% and increases when hydrate saturation was between 4.23% and 40.46%. The initial decrease in permeability was attributed to hydrate blockage of flow channels. They further stated that clay particles form aggregate structures during hydrate formation. The inter-aggregate spaces provide more conduits for gas flow, hence the increased permeability at high hydrate saturations. There was a critical hydrate saturation at which the effect of blockage and clay particle aggregation offset each other. At this point, the permeability to gas of the hydrate-bearing sediment equals to that of non-hydrate-bearing clayey sediments. Permeability measurement experiments were conducted with montmorillonite (Wu et al., 2018) and the observed results were similar to that observed with kaolin by Liu et al. (Liu et al., 2016).

Although great efforts were made to measure permeability of a variety of gas hydrate-bearing sediments, there is a paucity of information of the mechanisms behind the observed permeation behaviour aforementioned. Moreover, it is noted that the experiments reported in literature were all conducted at constant differential pressures. However, under in-situ conditions in the presence of confining pressure, fluid flow may not be achieved until the viscous force overcomes capillary sealing. The capillary sealing can be measured in terms of breakthrough pressure (Smith et al., 2005) which is the excess pressure of the non-wetting fluid phase at which the

wetting phase is displaced enough to create a continuous flow path for the non-wetting phase.

In this work, we experimentally explored the characteristics of gas permeation through three distinctive types of sedimentary cores under varying differential pressure, including silica sand packs, sand-clay cores, and a consolidated sandstone core sample. It was aimed at having a deep insight into the permeation-control mechanisms and when these mechanisms become a dominant factor for the gas flow through different sediments in the absence and presence of gas hydrates. The first two types of core samples would simulate unconsolidated hydrate-free and hydrate-bearing sediments. Addition of clay would also give us more insights regarding the influence of mineralogy and grain size distribution on the gas permeation characteristics. The effect of degree of consolidation and pore size distribution on the gas flow and permeability could also be investigated from the experiments carried on the consolidated sandstone core sample.

2. Experimental Section

2.1. Materials

Research-grade methane with certified purity of 99.995 vol. % was supplied by BOC Limited. Deionized water was produced by an integral water purification system (ELGA DV 25). Experiments were conducted on three different types of core samples: (i) 100 wt. % silica sand (from Fife, Scotland), (ii) 95 wt.% silica sand + 5 wt.% montmorillonite clay (from Sardinia, Italy), and (iii) a consolidated sandstone core sample (from Elgin, Scotland). The silica sand has a density of 2.64 g/cm^3, particle sizes ranging from 1.2 µm to 600 µm, and a mean diameter of 256.5 µm. The montmorillonite clay has a density of 2.7 g/cm^3, particle sizes ranging from 0.1 to 150 µm, and a mean diameter of 2.1 µm. The consolidated sandstone core sample has a grain density of 2.55 g/cm^3, pore sizes ranging from 0.1 to 300 µm, and a mean pore size of 66.8 µm.

2.2. Experimental apparatus

Figure 1 shows a schematic representation of the apparatus used for measuring gas permeability. The core holder is made up of a cylindrical high-pressure stainless steel vessel (maximum working pressure: 34.5 MPa) with 4 and 10.8 cm inner and outer diameters, respectively and a total length of 34 cm. For each end, there is a threaded stainless steel endcap, having a 1/8 in. diameter hole to serve as a connection for fluid inlet/outlet. The threads allow for the injected gas to be distributed to its entire inflow face, and collected from all parts of its outflow face. A Viton rubber sleeve with inner diameter of 4 cm and length of 19.5 cm is also fitted inside the vessel in order to appropriately hold the core samples and make a gas-tight seal on the cylindrical walls of the sample when applying a confining pressure. When placed in the core holder, the sample is connected to the both endcaps. Moreover, there are two ports provided on the body of the core holder, one midway through the length of the vessel to apply desired radial confining pressure and the other, near one end of the vessel to exert axial confining pressure, if needed.

A copper coil is wound around the core holder and connected to a cryostat (Grant LTC) for the cooling fluid circulation. The core holder is then completely immersed in a water bath which is insulated to minimize the heat exchange with the environment. A Quizix pump (SP-5200 Pump System) is also connected to the pressure port at the middle of the cell through valve V7 to inject confining fluid (water) into the confining fluid chamber in order to maintain a constant confining pressure.

For a typical permeability measurement experiment, methane is injected from the source cell into the core sample through the inlet valve V1 and leaves the sample through the outlet valve V3. It should be noted that methane is pre-cooled to the temperature of the system by passing through a 2 meter length of 1/8 in. pipe coil immersed in the water bath before entering the core sample. A back-pressure regulator connected to the exit line maintains the pore pressure of the sample at the

set point during permeability measurement. The gas exiting the back-pressure regulator flows into a gas meter to measure the flow rate at reference conditions of temperature and pressure under which the gas flow rate is measured, and then is vented to atmosphere. Two Quartzdyne pressure transducers (QS30K−B, Quartzdyne Inc., USA) with an accuracy of ±0.005 MPa are used to precisely measure the inlet and outlet pressures, respectively. A calibrated platinum-resistance thermometer (Pt100, supplied by TC Ltd.) with an accuracy of better than ± 0.1 K is also attached to the body of the vessel to measure the system temperature. Data from the pressure transducers, the thermometer, and the Quizix pump are acquired by a data acquisition system (DAS) and recorded on a PC with a LabVIEW software interface.

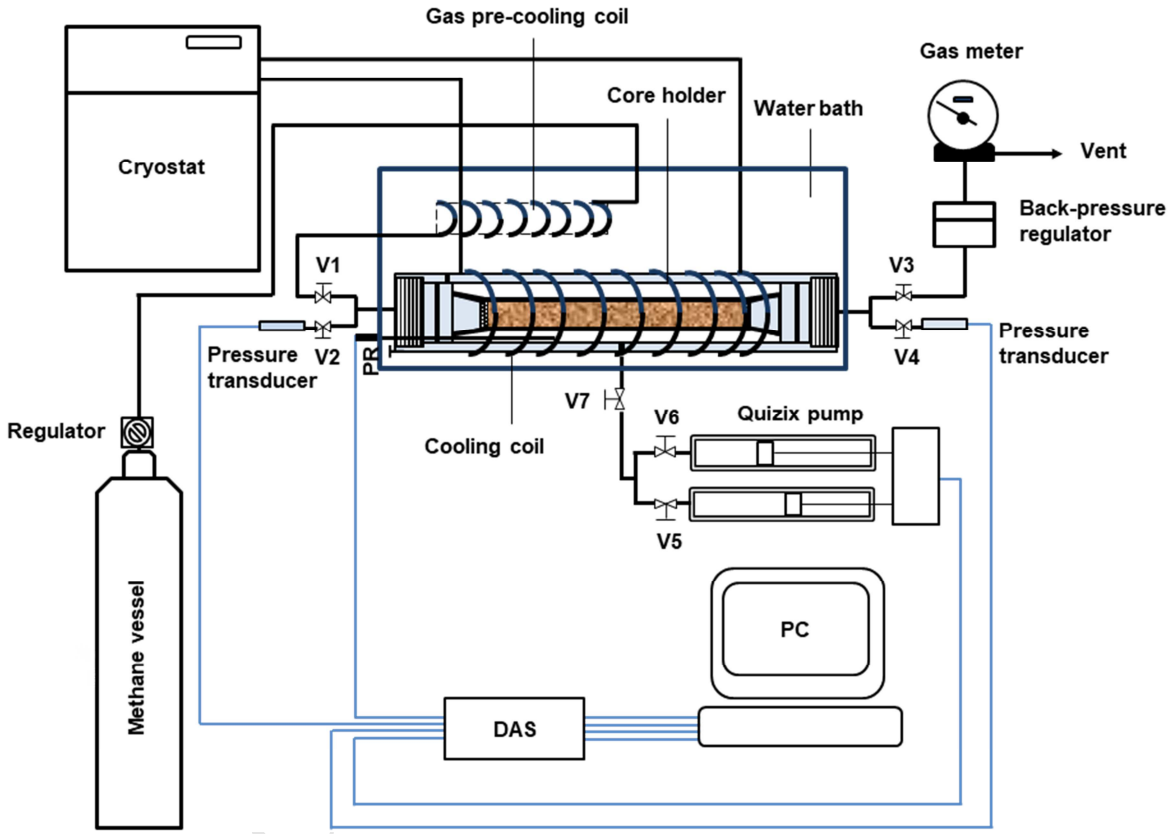

Figure 1 Schematic diagram of the experimental setup for permeability measurement: The blue lines represent cables for electrical communications while the black lines represent conduits for fluid flow.

2.3. Experimental procedure

2.3.1. Hydrate-free core samples

The sediment minerals were firstly dried in an oven at 343 K over 24 hours; then, a given quantity of which (100 wt. % silica sand or 95 wt. % silica sand + 5 wt. % montmorillonite) was thoroughly mixed and wetted with 14.3 wt. % of deionized water to obtain a homogeneous mixture. It should be noted that this is the procedure we follow to make our synthetic test specimens and the micro-textures of the sediment grains were visually examined in our previous works using ESEM to make

sure that particles are well mixed (Yang et al., 2019). The sample was then loaded into the sleeve in layers, and the desired packing was achieved using a cylindrical pestle rod. The core sample was placed into the vessel and the endcaps were positioned to hold the core sample in place and the vessel was immersed in the water bath and vacuumed.

Both the back-pressure regulator and the pressure regulator on the methane source cell were set to 3.45 MPa while the inlet and outlet valves (V1 and V3, respectively) were fully closed to disconnect the core sample from the gas source. Thereafter, the confining pressure was incrementally applied via the Quizix pump while allowing the gas injection to the core sample (by opening the inlet valve V1) until the pore pressure of the system reached 3.45 MPa and the confining pressure was 6.9 MPa. Throughout the experiments, the confining pressure was maintained at 3.45 MPa higher than the pore pressure of the system to ensure an appropriate sealing around the core sample and prevent bypassing of the gas. The inlet and outlet valves were then fully opened to allow for the gas flow. When steady-state conditions (constant flow rate and inlet/outlet pressures) were achieved, the gas flow rate measured at reference pressure (P_r) and temperature (T_r) together with inlet and outlet pressures were recorded for the calculation of the gas permeability according to Darcy's equation (See Eq.(6)). The permeability measurement was then repeated at different differential pressures by increasing the inlet pressure in steps. It should be noted that throughout the experiments, the inlet pressure was set sufficiently small to (i) permit use of the Darcy's equation for calculation of the gas permeability and (ii) keep water immobile to have only a single phase (gas) flow in the system. After each experiment, three samples were taken from the top, middle, and bottom of silica sand and silica sand-montmorillonite clay core samples and their water content was measured in order to ensure that water was homogeneously distributed and kept immobile during the test.

2.3.2. Hydrate-bearing core samples

The sediment core samples were prepared, packed and loaded to the high-pressure core holder following the similar procedure described in Section 2.3.1. Permeability of hydrate-bearing sediments to gas was measured for a series of methane hydrate saturation. For a typical methane hydrate saturation, while the outlet valve V3 was shut and the confining pressure kept at 3.45 MPa higher than the pore pressure using the Quizix pump, methane was injected into the core sample according to the desired pressure for hydrate formation. The system temperature was then set to 293 K and allowed to equilibrate over 24 hours. When the equilibrium was achieved, the system temperature was set to 273.7 K to initiate the methane hydrate formation. As the pore pressure decreased gradually due to the gas consumption for the hydrate formation, the confining pressure was also adjusted accordingly to maintain the 3.45 MPa pressure difference. This continued until the pressure change became insignificant signifying the completion of the hydrate formation. Upon the completion of the hydrate formation, the back-pressure regulator was set to 3.45 MPa to

maintain the constant pore pressure. For pore pressure in excess of 3.45 MPa after the hydrate formation, the excess gas was vented, and for pore pressure less than 3.45 MPa, gas was injected from the methane source cell. This ensured that the pore pressure was well above the methane hydrate equilibrium phase boundary at 273.7 K at which no hydrate dissociation occurred (See Appendix A). Afterwards, the inlet pressure was set to 3.45 MPa with the aid of the regulator on the methane source cell. The inlet and outlet valves were then closed to allow the system to attain pressure equilibrium. After the equilibrium was attained, both valves were fully opened for the gas flow through the core sample. When the steady state conditions were achieved, the gas flow rate was measured at P_r and T_r. The inlet and outlet pressures were also recorded for the calculation of the gas permeability according to Darcy's equation. Then, the inlet pressure was increased to measure the core sample permeability to gas at different differential pressures. The differential pressure exerted on the samples were also small enough to allow for use of Darcy's equation while keeping water phase in the system immobile and more importantly preventing hydrate formation/dissociation during the experiments.

2.4. Calculation of the saturations and permeability

The saturations of gas hydrate, water, and gas was calculated based on the real gas equation of state:

$$PV = ZnRT \tag{1}$$

where P, T, and V denote the pore pressure, system temperature, and gas volume, respectively. Z and n are the compressibility factor and the number of moles of methane gas, respectively. R is the gas constant.

The porosity of specimens was determined by gravimetric method:

$$\phi = 1 - \frac{M_s}{V_b \rho_s} \tag{2}$$

where ϕ is the porosity, M_s is the mass of the dry specimen, ρ_s is the average grain density of the sediment (i.e. a sum of the product of the weight fraction and the density of each mineral component), and V_b is the bulk volume of the specimen. After completion of the methane hydrate formation, the saturation of the methane hydrate, water, and gas were calculated using below equations:

$$S_h = \frac{V_h}{V_p} = \frac{\left(\frac{m_{CH_4}}{MW_{CH_4}} - \frac{PV}{ZRT}\right)\left(MW_{CH_4} + MW_w\gamma\right)}{V_p \rho_h} \tag{3}$$

$$S_w = \frac{V_w}{V_p} = \frac{V_{w0} - \left(\frac{m_{CH_4}}{MW_{CH_4}} - \frac{PV}{ZRT}\right)\frac{\gamma MW_w}{\rho_w}}{V_p} \tag{4}$$

$$S_g = 1 - S_h - S_w \tag{5}$$

in which S_h, S_w, and S_g represent hydrate saturation, water saturation, and gas saturation, respectively. V_h and V_p are the methane hydrate volume and pore volume, respectively. MW_{CH4} and MW_w are the molecular weight of methane and

367 water, respectively (MW_{CH4} = 16.04 g/mol and MW_w = 18.01 g/mol) and m_{CH4} is the
368 mass of the injected methane. γ is the hydration number and ρ_h is the bulk density of
369 the methane hydrate ($\gamma \cong 6.0$ and $\rho_h \cong 0.92$ g/cm^3) (Sloan Jr and Koh, 2007). V_w and
370 V_{w0} represent the water volume after and prior to the hydrate formation, respectively
371 and ρ_w is the density of water, 1.0 g/cm^3.
372 The gas permeability was calculated using Darcy's equation (RP40, 1998):

$$k_g = \frac{2\mu P_r q_r Z_m}{Z_r G_f (P_i^2 - P_o^2)} \quad (6)$$

373 where k_g is the permeability of the core sample to gas and P_i, P_o, and P_r, stand for
374 inlet pressure, outlet pressure, and the reference pressure at which the flow rate q_r
375 was measured, respectively. Z_r and Z_m are the methane compressibility factor at
376 reference and mean pore pressures, respectively. μ is the gas viscosity and G_f is the
377 geometric factor which for axial flow could be expressed by:

$$G_f = \frac{\pi D^2}{4L} \quad (7)$$

378 in which L and D are the core length and diameter, respectively.
379 The permeability of a porous medium to gas depends on the mean free path of the
380 flowing gas due to gas slippage pointed out by Klinkenberg. As presented by
381 Klinkenberg, gas permeability measured at several different mean pore pressures
382 could be extrapolated to infinite mean pore pressure using Eq.(8) to find the
383 Klinkenberg permeability, k_∞, which is equal to the permeability of the medium
384 obtained by a non-reactive fluid (RP40, 1998):

$$k_g = k_\infty \left(1 + \frac{b}{P_m}\right) \quad (8)$$

385 where b is the gas slippage factor and P_m is the mean pore pressure expressed by:

$$P_m = \frac{P_i + P_o}{2} \quad (9)$$

386 According to Eq.(8), it is expected for gas permeability to be linearly proportional with
387 the reciprocal of the mean pore pressure (Klinkenberg, 1941). It should be noted that
388 the difference between the permeability measured by gas becomes higher than that
389 measured by a non-reactive fluid when the medium permeability decreases. Further
390 discussion regarding the gas slippage and Klinkenberg effect can be found
391 elsewhere (RP40, 1998).
392

3. Results and Discussion

As mentioned before, two types of core samples composed of 100 wt. % silica sand and 95 wt. % silica sand + 5 wt. % montmorillonite clay were used to simulate unconsolidated hydrate-free and hydrate-bearing sediments. Addition of 5 wt. % montmorillonite was to enable us to investigate the effect of sediment mineralogy on gas flow. The third series of experiments was conducted on a consolidated sandstone core sample to study the effect of the degree of consolidation and pore size distribution on gas flow and permeability. Table 1 summarizes the properties and the initial parameters of the core samples before the permeability measurements.

Table 1 Properties and parameters of the sediment core samples

Sedimentary mineral	Core sample	Initial porosity (%)	Saturation (vol. %)		
			S_h	S_g	S_w
100 wt. % Silica sand	1	40.0	0	32.1	67.9
	2	40.3	17.6	42.9	39.5
	3	40.3	22.7	42.5	34.8
	4	40.6	40.3	41.8	17.9
	5	40.3	59.7	39.6	0.7
95 wt. % Silica sand + 5 wt. % Montmorillonite	6	36.2	0	33.6	66.4
	7	36.2	22.9	30.1	47.0
	8	34.5	28.1	23.8	48.1
	9	36.2	35.0	27.5	37.5
Consolidated sandstone	10	18.2	0	45.0	55.0
	11	18.2	15.0	45.0	40.0
	12	18.2	44.0	45.0	11.0

3.1. Permeability of silica sand core samples

The sand packs were 155 mm in length and 38.1 mm in diameter. Gas permeability was measured at five different methane hydrate saturations (S_h): 0, 17.6, 22.7, 40.3, and 59.7. The measured permeability values are shown in Figure 2.

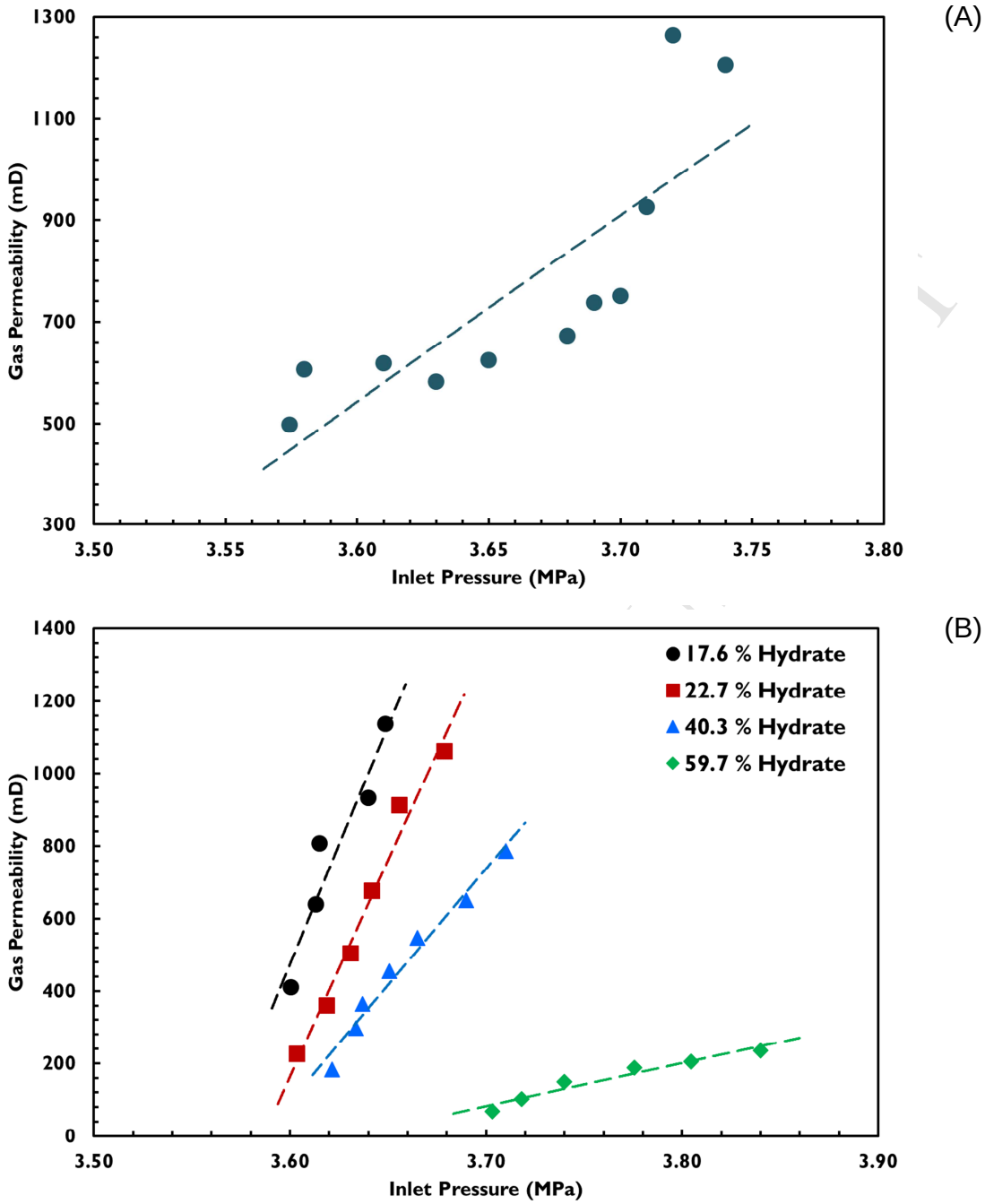

Figure 2 Gas permeability of sand packs against the inlet pressure: (A) hydrate-free sand pack, (B) hydrate-bearing sand pack at different saturations of methane hydrate. As shown, the gas permeability behaviour is mainly dominated by the breakthrough capillary pressure

In Figure 2-(A), the gas permeability for both hydrate-free and hydrate-bearing samples increases with the inlet pressure and accordingly mean pore pressure given that the outlet pressure of the system was maintained at 3.4 MPa, apparently opposite of what would be expected according to Klinkenberg effect (See Eq.(8)). On one hand, the silica sand has coarse grains (average size of 256.5 μm), leading to large intergranular pore spaces in its packs hence the reduced restriction to flow. On the other hand, Klinkenberg effect is expected to be less influential on the gas permeability in high-permeable media. Therefore, the measured gas permeability is weakly affected by Klinkenberg effect. Instead, owing to the dominance of viscous

forces over the capillary forces on pathways previously filled with water, particularly those critical narrow ones, more contribution to the gas flow occurs as the inlet pressure hence the differential pressure increase.

As observed in Figure 2-(B), since methane hydrate forms in the pores, preferably in the large ones, the restrictions to the fluid flow gradually increases, causing reduction in the permeability of the medium, which its severity strongly depends on the pore-scale growth habits of hydrates. This observation is also corroborated by the differential pressure at gas breakthrough which was 0.151, 0.154 and 0.172 MPa for 17.6, 22.7 and 40.3 % hydrate saturations, respectively; then, at 59.7 %, the differential pressure at gas breakthrough was 0.253 MPa confirming the strong impact of the pore-scale habits of methane hydrate on the permeability of the host sediment. In fact, pore-scale habits altered from the pore-filling to the cementation at hydrate saturations higher than 50 %, having two main consequences:

1. When more hydrates form in the pore spaces, the size of the remaining pores available for the fluid flow becomes smaller, resulting in a higher capillary sealing hence higher breakthrough pressure to initiate the gas flow. Therefore, one can conclude that the breakthrough capillary pressure plays a dominant role in the permeability of the coarse sand packs.
2. At higher hydrates saturations hence lower water saturations, the sand grains become cemented and consolidated by the hydrates, creating more pore-throats and making channels critically contributing to the gas flow narrower. Therefore, it would result in Klinkenberg effect to be more influential. This is confirmed by changes in the slopes of gas permeability values versus the inlet pressure at different hydrate saturations.

It should be noted that the permeability measurement for 22.7 % methane hydrate saturation was conducted first with increasing the inlet pressure and then in a reverse manner with decreasing the inlet pressure. It can be seen from Figure 3 that the permeability profile in both cases follows identical patterns. This repeatability evidently supports our assumption that the pore water in the core sample remained immobile throughout the experiments and its re-distribution does not have measurable effect on the gas permeability, given that a typical gas velocity is less than 5 cm/s. Furthermore, it confirms that the inlet pressure was sufficiently set near HSZ of methane hydrate so that there was no hydrate formation/dissociation, thus the hydrate saturation did not change during permeability measurement.

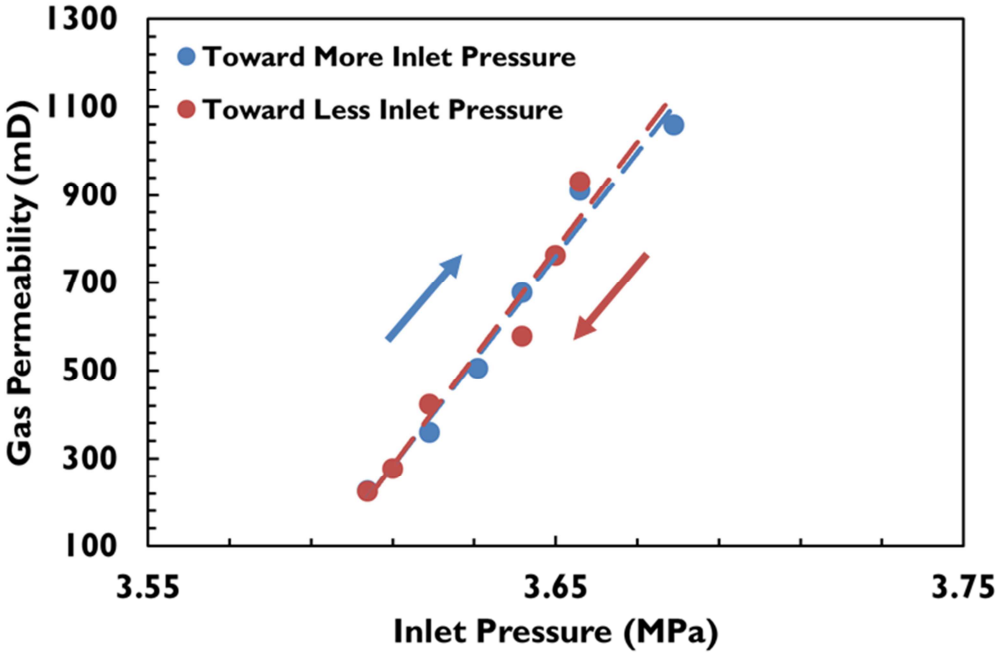

Figure 3 Gas permeability of sand packs with 22.7 % methane hydrate saturation measured firstly toward higher inlet pressure and then in a reverse manner. The measured gas permeability trends have an acceptable agreement with each other, confirming no measurable hydrate formation/dissociation and water outflow during the experiments.

3.2. Permeability of silica sand-montmorillonite clay core samples

In order to investigate the effect of the grain mineralogy and pore size on the gas permeation, 5 wt. % montmorillonite clay was added to the silica sand. The core sample dimensions were the same as those of the silica sand core samples. Gas permeability was measured at four different methane hydrate saturations of 0, 22.9, 28.1, and 35.0 and the results are indicated in Figure 4. As can be seen, the medium permeability to the gas is considerably impacted due to the presence of the clay.

As shown in Figure 4-(A), the fine grain particles of the clay (with mean grain size of 2.1 μm) could fill in the large pore spaces and form fine pore-dominated sediments. As a consequence, the gas permeation behaviour through the sand-clay core sample is significantly different from those obtained for the silica sand core sample (See Figure 2-(A)). The silica sand has a large particle size hence large intergranular and interconnected pore spaces due to higher resistance to compaction. Thus, the restriction to the gas flow is relatively small and Klinkenberg effect is not influential. However, for the case of the sand-clay sample, fine clay particles play an important role in reducing the pore-throat sizes hence highlighting Klinkenberg effect. This can be simply justified according to the fact that the montmorillonite clay particles in the large pores of the silica sand form fine channels for the gas flow, which become more significant, given that montmorillonite clay could swell greatly after absorbing water because montmorillonite is a strong absorbent of water (Aksu et al., 2015). In

such fine pores, the gas slippage is expected to occur and the behaviour of the gas permeability becomes mainly dominated by Klinkenberg effect rather than breakthrough capillary pressure. Therefore, it can be seen here that the gas permeability of the sediments decreases as the inlet pressure increases.

Figure 4-(B) shows that the presence of methane hydrate significantly changed the gas permeation behaviour in the sand-clay core samples. First of all, the permeability of the hydrate-free sand-clay core sample is up to two orders of magnitude higher than those with methane hydrate. This is simply understood because gas hydrates prefer to form in large pore spaces (Priest et al., 2009; Tohidi et al., 2001), therefore, tend to substantially reduce the pore size, resulting in severe restrictions for the fluid flow (Minagawa et al., 2008).

Next, it is interesting to observe that the higher saturations of methane hydrate led to higher gas permeability for the hydrate-bearing sand-clay core samples, which is apparently in contrast with most of the other works reported in literature. Similar observation was also reported by Wu et al. (Wu et al., 2018). For the three tests with a certain saturation of hydrate, after most of the limited large pores were blocked by hydrate crystals, further more hydrate crystals could act as coarse grains pushing apart the sediment grains hence enlarging the sediment pores (Waite et al., 2009), a phenomenon known as hydrate-forced heave. This phenomenon led to the increase in the sediment porosity and as a consequence, gas permeability as the hydrate saturation increased (Cook et al., 2008) by altering the pore structures of the sediments, similar to the clay in soils (Barden et al., 1972). Once the hydrate saturation becomes above a critical value, agglomeration could be dominant over pore clogging. The hydrate crystals could aggregate fine clay particles and form inter-aggregation pores (macro pores) that are considerably larger than the inter-particle pores (micro pores) (Zdravkov et al., 2007). If the above assumptions are true, it could be anticipated that there should be a critical hydrate saturation for a specific porous medium according to its grain types and size distribution. When the hydrate saturation is smaller than it, hydrate formation will significantly reduce the permeability by clogging pores; once the hydrate saturation becomes higher than that, hydrate-forced heave or aggregating will dominate the effect on permeability. This anticipation could also be validated through comparing the gas permeability behaviour of the hydrate-bearing sand-clay core samples with those of silica sand samples (See Figure 2-(B)). However, further investigation is required in this regard.

The third particularity is the non-monotonous change of the gas permeability against the inlet pressure. The gas permeability increased initially, then gradually decreased after reaching a maximum value as the inlet pressure increased. This observation may be attributed to two underlying processes. The first possible reason could be hydrate-forced heave, as discussed before; the growth of hydrate crystals may slightly push apart sediment grains, enlarging channels for the gas flow, in which the capillary sealing plays an important role in the permeability. At the beginning, increase in the inlet pressure broke through more enlarged capillary pores, therefore,

leading to increase in the gas permeability. As can also be seen in Figure 4-(B), the breakthrough capillary pressure is lower for the sand-clay core sample with higher methane hydrate saturation. This is agreeable with the previous discussion that higher saturation of methane hydrate resulted in severe effect of hydrate-forced heave on the pores of the sand-clay core samples, whilst the presence of methane hydrate resulted in contrary effect on the breakthrough capillary pressure of the sand cores. Moreover, the capillary breakthrough process created more change in the permeability for the core sample with more methane hydrate, further supporting the hydrate-forced heave assumption. The maximum values are 0.27, 0.62, and 1.79 mD for 22.9, 28.1, and 35.0 % hydrate saturations, respectively. Beyond the maximum point, a majority of the large pores that had been created by hydrate-forced heave were already broken through; therefore, the gas flow is no longer capillary dominated but the viscous dominated. Thus, gas slippage occurred and Klinkenberg effect became significant, leading to gradual decrease in the measured permeability as the inlet pressure increased further.

(A)

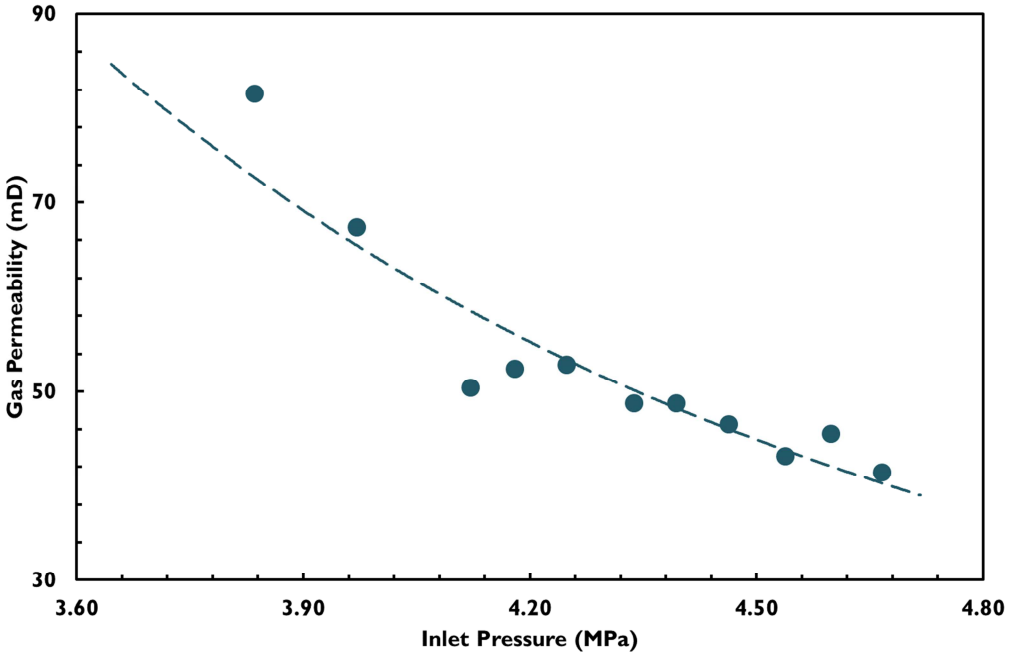

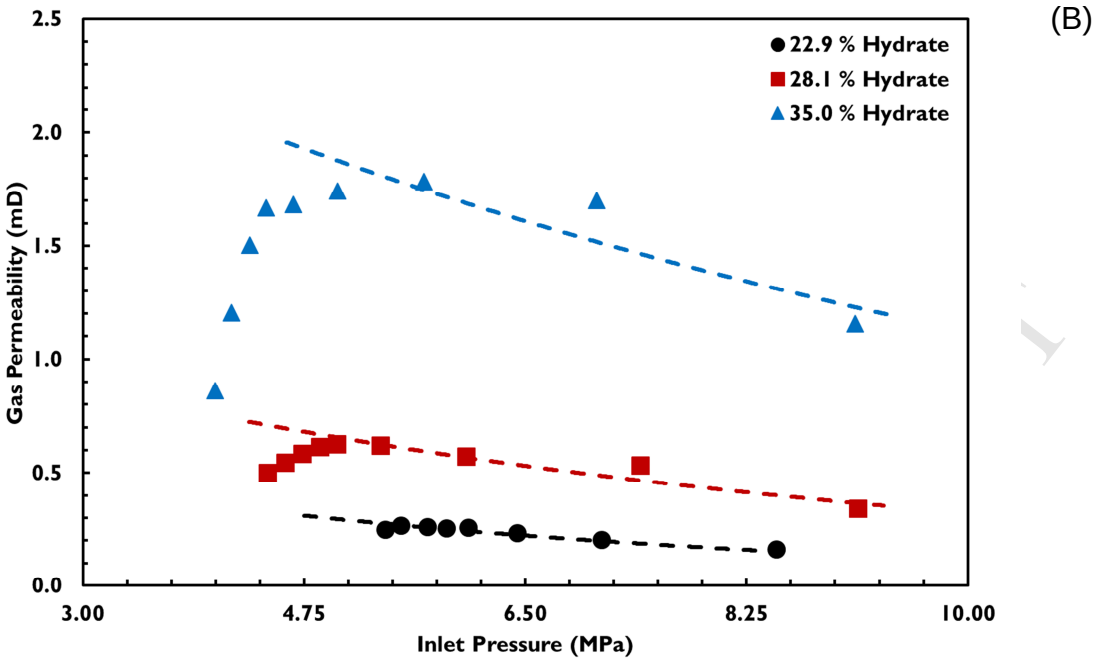

Figure 4 Gas permeability of the sand-clay core samples versus the inlet pressure: (A) hydrate-free sample, (B) hydrate-bearing samples with different saturations of methane hydrate

3.3. Permeability of consolidated sandstone core sample

Permeability of a consolidated sandstone core sample to gas was also measured to investigate how the presence of gas hydrates affect the gas permeation characteristics through well-consolidated porous media where the mineralogical grains are immobile compared with two previous cases studies. The sandstone core sample was made in dimensions similar to the unconsolidated cores to be able to fit in the same rubber sleeve, 155 mm in length and 38.1 mm in diameter.

Figure 5 shows the measured gas permeability of the sandstone core sample for both hydrate-free and hydrate-bearing cases. As observed in Figure 5-(A), the gas permeability increases with increasing the inlet pressure, similar to that observed for the unconsolidated silica sand core sample in Figure 2-(A). This means the pores of the sandstone core sample were large enough that the capillary breakthrough dominated the gas slippage phenomenon. However, the orders of magnitude of the measured permeability are different, which can be simply understood by having a look at the porosity values, given the permeability and porosity of a medium are generally proportional to each other.

As indicated in Figure 5-(B), the presence of methane hydrate resulted in the gas permeability to be severely reduced. Moreover, since the sandstone core sample was well-consolidated, no hydrate-forced heave occurred. Therefore, in contrast to the observations for the sand-clay samples, the higher the hydrate saturation, the lower the porous medium permeability to methane. It can also be seen that the presence of methane hydrate altered the response of the gas permeability to the

pressure change, i.e. the permeability decreased with increasing the inlet pressure, then approaching a relative constant value as the inlet pressure continuously increased. This could be attributed to the fact that the methane hydrate crystals preferably occupied the large pores, either fully blocking the large pores or partially clogging them and forming fine throat channels. As observed in Figure 5-(B), much higher inlet pressure was required to be able to break through the capillary pressure in the hydrate-bearing cases than that in the absence of hydrate, evidently supporting the assumption that formation of methane hydrate transformed the large pores into fine channels for the gas flow where the collision of methane gas molecules with the pore walls could result in the gas slippage to occur and consequently Klinkenberg effect to be dominant.

The gas permeability measurement for the 15.0 % hydrates saturation was carried out first with increasing the inlet pressure and then in a reverse manner to check the repeatability of the experimental results. As brought in Figure 6, the measurements were repeatable, confirming that the re-distribution of the pore water had no significant influence on the permeability under the experimental conditions.

(A)

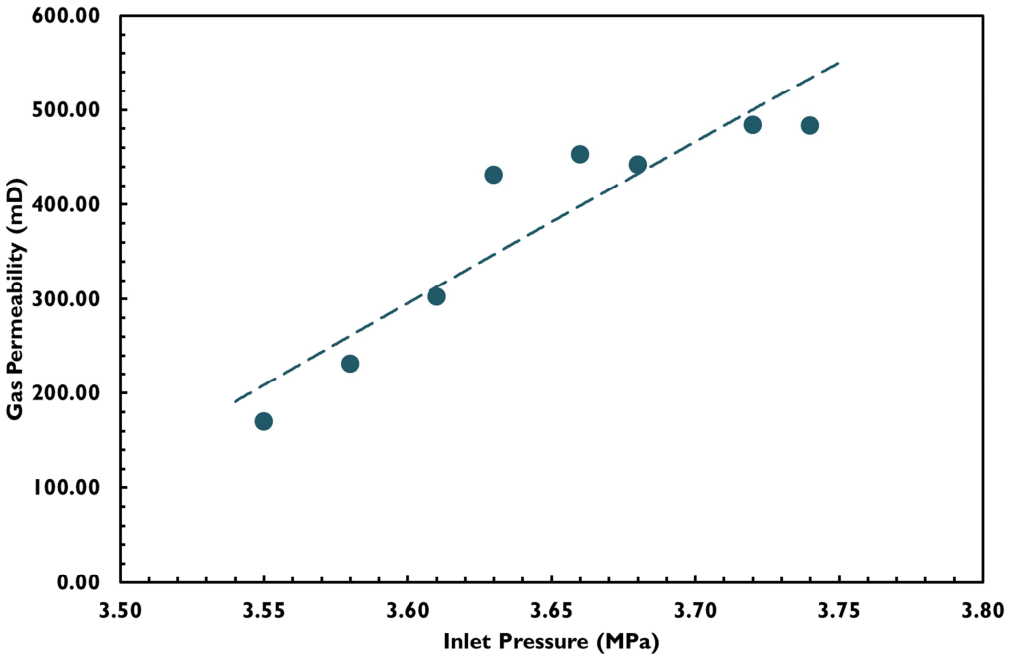

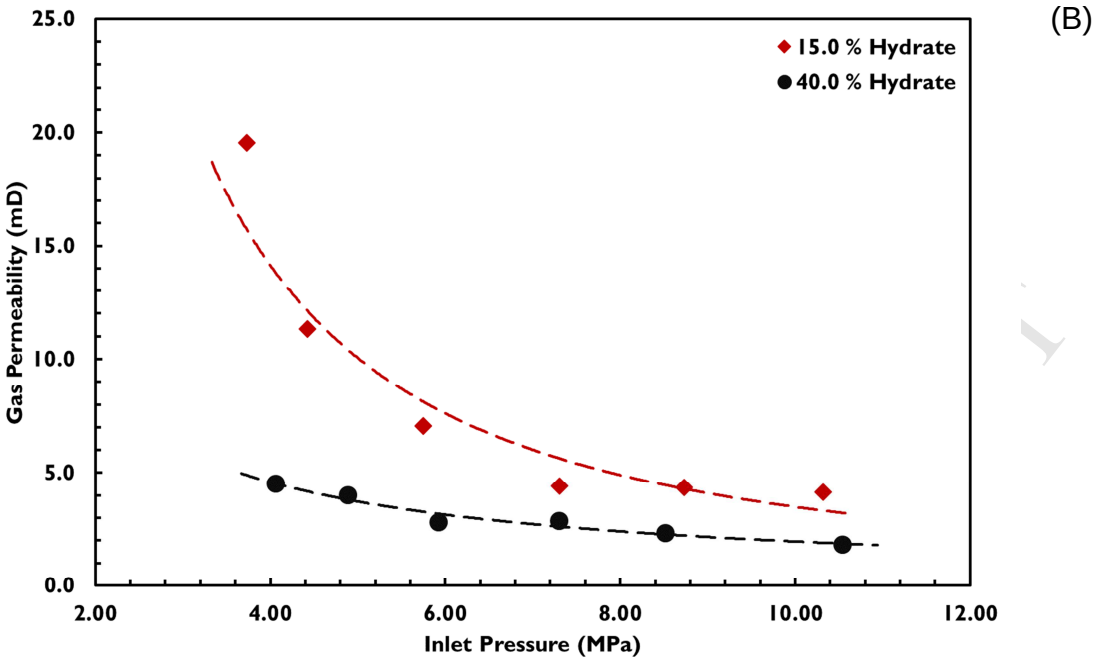

581 Figure 5 Gas permeability of the consolidated core samples versus the inlet pressure: (A)
582 hydrate-free sample, (B) hydrate-bearing samples with different saturations of methane
583 hydrate

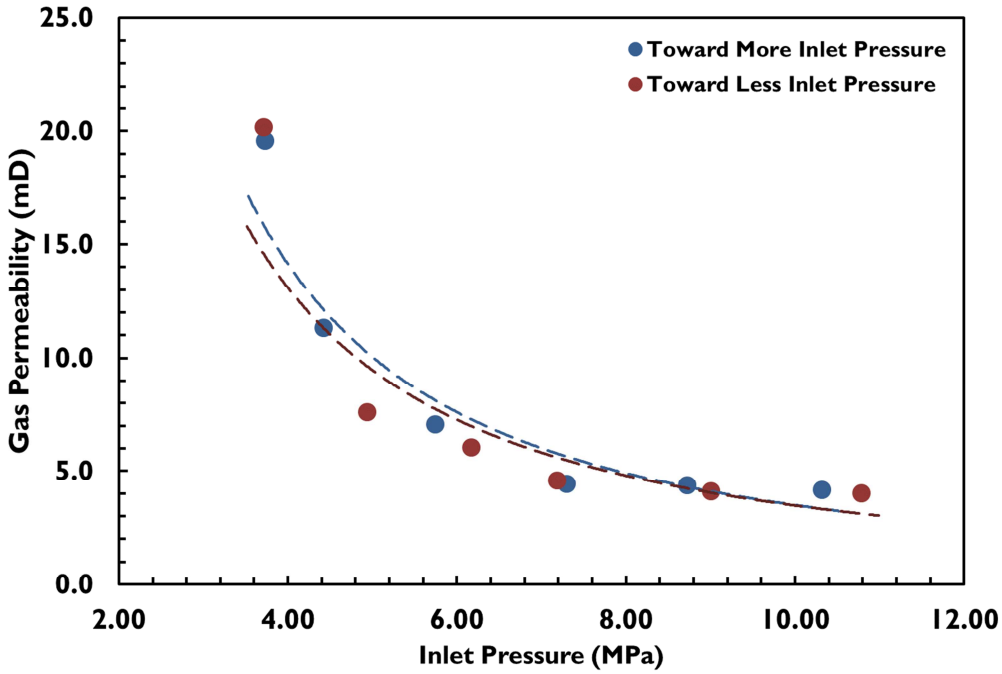

584

585 Figure 6 Gas permeability of the consolidated core samples with 15.0 % methane hydrate
586 saturation measured firstly toward higher inlet pressure and then in a reverse manner

587

588

4. Conclusions

Gas permeability was measured under varying differential pressure for three different types of sedimentary core samples to investigate gas permeation characteristics in the presence and absence of natural gas hydrates. The experimental results showed that the gas permeation at different gas hydrate-bearing sediments could be dominated by different mechanisms including capillary breakthrough, pore/grain size distribution, hydrate clogging, hydrate-forced heave or agglomeration, and Klinkenberg effect. The following conclusions can be drawn from this study:

- For the highly porous and permeable silica sand core samples, it was observed that the gas permeability increases with increasing the inlet pressure hence differential pressure in both hydrate-free and hydrate-bearing cases, due to dominance of the capillary breakthrough mechanism over the gas slippage. As the viscous force dominates the breakthrough capillary forces, the contribution to the gas flow from the narrower pathways previously filled with water becomes highlighted, resulting in lower resistance against the flow. As also expected, gas hydrate formation adversely affected the permeability of the medium. Depending on the hydrate saturation and pore-scale habits, the permeability of the sand pack was reduced. However, the pore sizes were still large enough to keep the breakthrough capillary pressure mechanism dominant and Klinkenberg effect negligible.

- For the sand-clay core samples containing 5 wt. % montmorillonite, due presence of fine clay particles swelled by water in large pores, the pathways available for the gas flow was reduced or became narrower and the gas permeability of the porous medium was dominated by Klinkenberg effect. Therefore, the gas permeation characteristics for this sedimentary sample became different from the silica sand pack. It was also observed that the effect of the hydrate formation on the gas permeability for the sand-clay samples is drastic given that hydrates prefer to form in large pores. More interestingly, due to the hydrate-forced heave phenomenon, the measured gas permeability values were higher for the higher methane hydrate saturations. In addition, the gas permeability behaviour for all hydrate saturations was ascending at lower inlet pressures due to dominance of hydrate-forced heave and then descending at higher inlet pressures due to dominance of Klinkenberg effect.

- For the consolidated sandstone core sample, gas permeation characteristics were considerably altered. For the hydrate-free case, the breakthrough capillary pressure dominated the gas permeation so that the gas permeability increased with the inlet pressure, similar to that of the unconsolidated silica sand packs. However, hydrate formation clogged the original large pores thus resulted in the gas slippage to be influential, resulting in Klinkenberg effect to

631 be dominant. Therefore, for the hydrate-bearing cases, the gas permeability
632 was reduced with increasing the inlet pressure. Moreover, in contrast to the
633 sand-clay core samples, no hydrate-forced heave effect was indicated by the
634 gas permeability trend given well-consolidation of the sandstone core sample.

5. Acknowledgements

This work was financially supported by the Skolkovo Institute of Science and Technology, Russia, which is acknowledged.

Appendix A

We used our in-house thermodynamic modelling software to predict the hydrate stability zone (HSZ) of CH_4 (Hassanpouryouzband et al., 2018a). Thermodynamic behaviour of the fluid system at different thermodynamic conditions and compositions was modelled using CPA EoS for the non-solid phase, with the SRK72 EoS as the no associating part, and a modified VdW-Platteeuw method for the solid phase.

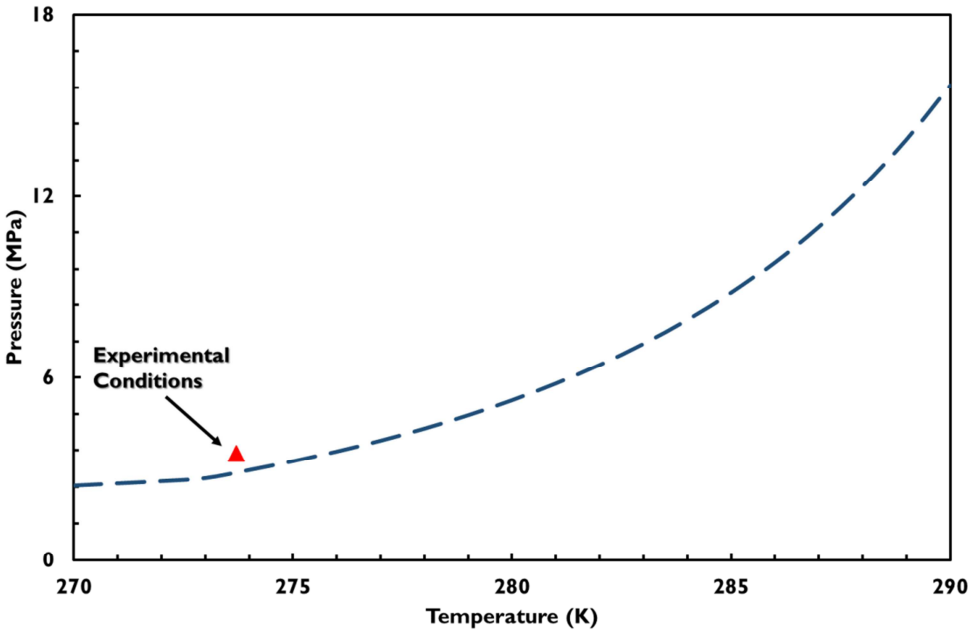

Figure A1 Predicted hydrate stability zone (HSZ) of CH_4 and experimental conditions

6. References

Aksu, I., Bazilevskaya, E., Karpyn, Z.T., 2015. Swelling of clay minerals in unconsolidated porous media and its impact on permeability. GeoResJ 7, 1–13.

Barden, L., Madedor, A.O., Sides, G.R., 1972. The flow of air and water in partly saturated clay soil, in: Developments in Soil Science. Elsevier, pp. 299–311.

Castaldi, M.J., Zhou, Y., Yegulalp, T.M., 2007. Down-hole combustion method for gas production from methane hydrates. J. Pet. Sci. Eng. 56, 176–185.

Chen, X., Verma, R., Espinoza, D.N., Prodanović, M., 2018. Pore-Scale Determination of Gas Relative Permeability in Hydrate-Bearing Sediments Using X-Ray Computed Micro-Tomography and Lattice Boltzmann Method. Water Resour. Res. 54, 600–608.

Choi, J., Dai, S., Cha, J., Seol, Y., 2014. Laboratory formation of noncementing hydrates in sandy sediments. Geochemistry, Geophys. Geosystems 15, 1648–1656.

Collett, T.S., 1992. Potential of gas hydrates outlined. Oil Gas Journal;(United States) 90.

Cook, A.E., Goldberg, D., Kleinberg, R.L., 2008. Fracture-controlled gas hydrate systems in the northern Gulf of Mexico. Mar. Pet. Geol. 25, 932–941.

Daigle, H., 2016. Relative permeability to water or gas in the presence of hydrates in porous media from critical path analysis. J. Pet. Sci. Eng. 146, 526–535.

Delli, M.L., Grozic, J.L.H., 2014. Experimental determination of permeability of porous media in the presence of gas hydrates. J. Pet. Sci. Eng. 120, 1–9.

Dickens, G.R., O'Neil, J.R., Rea, D.K., Owen, R.M., 1995. Dissociation of oceanic methane hydrate as a cause of the carbon isotope excursion at the end of the Paleocene. Paleoceanogr. Paleoclimatology 10, 965–971.

Falser, S., Uchida, S., Palmer, A.C., Soga, K., Tan, T.S., 2012. Increased gas production from hydrates by combining depressurization with heating of the wellbore. Energy & fuels 26, 6259–6267.

Fitzgerald, G.C., Castaldi, M.J., 2013. Thermal stimulation based methane production from hydrate bearing quartz sediment. Ind. Eng. Chem. Res. 52, 6571–6581.

Fu, W., Wang, Z., Sun, B., Chen, L., 2018. A mass transfer model for hydrate formation in bubbly flow considering bubble-bubble interactions and bubble-hydrate particle interactions. Int. J. Heat Mass Transf. 127, 611–621.

Fu, W., Wang, Z., Sun, B., Ji, C., Zhang, J., 2019. Multiple controlling factors for methane hydrate formation in water-continuous system. Int. J. Heat Mass Transf. 131, 757–771.

Hassanpouryouzband, A., Vasheghani Farahani, M., Yang, J., Tohidi, B., Chuvilin, E., Istomin, V., Bukhanov, B.A., 2019a. Solubility of Flue Gas or Carbon Dioxide-Nitrogen Gas Mixtures in Water and Aqueous Solutions of Salts: Experimental Measurement and Thermodynamic Modelling. Ind. Eng. Chem. Res.

Hassanpouryouzband, A., Yang, J., Joonaki, E., Tohidi, B., Chuvilin, E., Bukhanov, B., Istomin, V., 2017. A Novel Method for CO2 Storage and Methane Recovery in Gas Hydrate Reservoirs through Injection of Flue Gas From Coal-fired Power Plants, in: 79th EAGE Conference and Exhibition 2017.

Hassanpouryouzband, A., Yang, J., Tohidi, B., Chuvilin, E., Istomin, V., Bukhanov, B., Cheremisin, A., 2018a. CO2 Capture by Injection of Flue Gas or CO2–N2 Mixtures into Hydrate Reservoirs: Dependence of CO2 Capture Efficiency on

Gas Hydrate Reservoir Conditions. Environ. Sci. Technol. 52, 4324–4330.
Hassanpouryouzband, A., Yang, J., Tohidi, B., Chuvilin, E., Istomin, V., Bukhanov, B., Cheremisin, A., 2018b. Insights into CO2 Capture by Flue Gas Hydrate Formation: Gas Composition Evolution in Systems Containing Gas Hydrates and Gas Mixtures at Stable Pressures. ACS Sustain. Chem. Eng. 6, 5732–5736.
Hassanpouryouzband, A., Yang, J., Tohidi, B., Chuvilin, E.M., Istomin, V., Bukhanov, B.A., 2019b. Geological CO2 Capture and Storage with Flue Gas Hydrate Formation in Frozen and Unfrozen Sediments: Method Development, Real Time-Scale Kinetic Characteristics, Efficiency, and Clathrate Structural Transition. ACS Sustain. Chem. Eng. https://doi.org/10.1021/acssuschemeng.8b06374
Holder, G.D., Kamath, V.A., Godbole, S.P., 1984. The potential of natural gas hydrates as an energy resource. Annu. Rev. Energy 9, 427–445.
Kang, H., Koh, D.-Y., Kim, D., Park, J., Cha, M., Lee, H., 2012. Recovery of Methane Intercalated in Natural Gas Hydrate Sediments Using a Carbon Dioxide and Flue Gas Mixture, in: The Twenty-Second International Offshore and Polar Engineering Conference. International Society of Offshore and Polar Engineers.
Kang, H., Koh, D.-Y., Lee, H., 2014. Nondestructive natural gas hydrate recovery driven by air and carbon dioxide. Sci. Rep. 4, 6616.
Kleinberg, R.L., Flaum, C., Griffin, D.D., Brewer, P.G., Malby, G.E., Peltzer, E.T., Yesinowski, J.P., 2003. Deep sea NMR: Methane hydrate growth habit in porous media and its relationship to hydraulic permeability, deposit accumulation, and submarine slope stability. J. Geophys. Res. Solid Earth 108.
Klinkenberg, L.J., 1941. The permeability of porous media to liquids and gases, in: Drilling and Production Practice. American Petroleum Institute.
Kneafsey, T.J., Seol, Y., Gupta, A., Tomutsa, L., 2011. Permeability of laboratory-formed methane-hydrate-bearing sand: measurements and observations using X-ray computed tomography. SPE J. 16(01), 78–94.
Kumar, A., Maini, B., Bishnoi, P.R., Clarke, M., Zatsepina, O., Srinivasan, S., 2010. Experimental determination of permeability in the presence of hydrates and its effect on the dissociation characteristics of gas hydrates in porous media. J. Pet. Sci. Eng. 70, 114–122.
Kvenvolden, K.A., 1988. Methane hydrate—a major reservoir of carbon in the shallow geosphere? Chem. Geol. 71, 41–51.
Li, B., Li, X.-S., Li, G., Feng, J.-C., Wang, Y., 2014. Depressurization induced gas production from hydrate deposits with low gas saturation in a pilot-scale hydrate simulator. Appl. Energy 129, 274–286.
Li, G., Wu, D.-M., Li, X.-S., Lv, Q.-N., Li, C., Zhang, Y., 2017. Experimental measurement and mathematical model of permeability with methane hydrate in quartz sands. Appl. Energy 202, 282–292.
Linga, P., Haligva, C., Nam, S.C., Ripmeester, J.A., Englezos, P., 2009a. Recovery of methane from hydrate formed in a variable volume bed of silica sand particles. Energy & Fuels 23, 5508–5516.
Linga, P., Haligva, C., Nam, S.C., Ripmeester, J.A., Englezos, P., 2009b. Gas hydrate formation in a variable volume bed of silica sand particles. Energy & Fuels 23, 5496–5507.
Liu, W., Wu, Z., Li, Y., Song, Y., Ling, Z., Zhao, J., Lv, Q., 2016. Experimental study on the gas phase permeability of methane hydrate-bearing clayey sediments. J. Nat. Gas Sci. Eng. 36, 378–384.
Loh, M., Too, J.L., Falser, S., Linga, P., Khoo, B.C., Palmer, A., 2014. Gas

production from methane hydrates in a dual wellbore system. Energy & Fuels 29, 35–42.
Long, D., Lovell, M.A., Rees, J.G., Rochelle, C.A., 2009. Sediment-hosted gas hydrates: new insights on natural and synthetic systems. Geol. Soc. London, Spec. Publ. 319, 1–9.
Masuda, Y., Maruta, H., Naganawa, S., Amikawa, K., Nagao, J., Hironori, H., Konno, Y., 2011. Methane recovery from hydrate-bearing sediments by N2–CO2 gas mixture injection: experimental investigation on CO2–CH4 exchange ratio, in: Proceedings of the 7th International Conference on Gas Hydrates, Edinburgh, Scotland, United Kingdom.
Max, M.D., Johnson, A.H., 2018. Exploration and Production of Oceanic Natural Gas Hydrate: Critical Factors for Commercialization. Springer.
Mehrabian, H., Bellucci, M.A., Walsh, M.R., Trout, B.L., 2018. Effect of Salt on Antiagglomerant Surface Adsorption in Natural Gas Hydrates. J. Phys. Chem. C 122, 12839–12849.
Minagawa, H., Nishikawa, Y., Ikeda, I., Sakamoto, Y., Miyazaki, K., Takahara, N., Komai, T., Narita, H., 2008. Relation between permeability and pore-size distribution of methane-hydrate-bearing sediments, in: Offshore Technology Conference. Offshore Technology Conference.
Moridis, G.J., Kowalsky, M.B., Pruess, K., 2009. TOUGH+ HYDRATE v1. 1 user's manual: a code for the simulation of system behavior in hydrate-bearing geologic media: Lawrence Berkeley National laboratory. Berkeley, CA.
Nakoryakov, V.E., Misyura, S.Y., Elistratov, S.L., Manakov, A.Y., Shubnikov, A.E., 2013. Combustion of methane hydrates. J. Eng. Thermophys. 22, 87–92.
Nimblett, J., Ruppel, C., 2003. Permeability evolution during the formation of gas hydrates in marine sediments. J. Geophys. Res. Solid Earth 108.
Ohgaki, K., Takano, K., Sangawa, H., Matsubara, T., Nakano, S., 1996. Methane Exploitation by Carbon Dioxide from Gas Hydrates—Phase Equilibria for CO2-CH4 Mixed Hydrate System—. J. Chem. Eng. Japan 29, 478–483.
Okwananke, A., Yang, J., Tohidi, B., Chuvilin, E., Istomin, V., Bukhanov, B., Cheremisin, A., 2018. Enhanced depressurisation for methane recovery from gas hydrate reservoirs by injection of compressed air and nitrogen. J. Chem. Thermodyn. 117, 138–146.
Priest, J.A., Rees, E.V.L., Clayton, C.R.I., 2009. Influence of gas hydrate morphology on the seismic velocities of sands. J. Geophys. Res. solid earth 114.
RP40, A.P.I., 1998. Recommended practices for core analysis. Feb.
Sakamoto, Y., Komai, T., Miyazaki, K., Tenma, N., Yamaguchi, T., Zyvoloski, G., 2010. Laboratory-scale experiments of the methane hydrate dissociation process in a porous media and numerical study for the estimation of permeability in methane hydrate reservoir. J. Thermodyn. 2010.
Scheidegger, A., 1958. The physics of flow through porous media. University Of Toronto Press: London.
Schicks, J., Spangenberg, E., Giese, R., Luzi-Helbing, M., Priegnitz, M., Beeskow-Strauch, B., 2013. A counter-current heat-exchange reactor for the thermal stimulation of hydrate-bearing sediments. Energies 6, 3002–3016.
Schoderbek, D., Martin, K.L., Howard, J., Silpngarmlert, S., Hester, K., 2012. North slope hydrate fieldtrial: CO2/CH4 exchange, in: OTC Arctic Technology Conference. Offshore Technology Conference.
Sloan Jr, E.D., 2003. Fundamental principles and applications of natural gas hydrates. Nature 426, 353.

Sloan Jr, E.D., Koh, C., 2007. Clathrate hydrates of natural gases. CRC press.
Smith, J.D., Chatzis, I., Ioannidis, M.A., 2005. A new technique to measure the breakthrough capillary pressure. J. Can. Pet. Technol. 44.
Spangenberg, E., Kulenkampff, J., Naumann, R., Erzinger, J., 2005. Pore space hydrate formation in a glass bead sample from methane dissolved in water. Geophys. Res. Lett. 32.
Sun, Y.-F., Zhong, J.-R., Li, R., Zhu, T., Cao, X.-Y., Chen, G.-J., Wang, X.-H., Yang, L.-Y., Sun, C.-Y., 2018. Natural gas hydrate exploitation by CO 2/H 2 continuous Injection-Production mode. Appl. Energy 226, 10–21.
Tohidi, B., Anderson, R., Clennell, M. Ben, Burgass, R.W., Biderkab, A.B., 2001. Visual observation of gas-hydrate formation and dissociation in synthetic porous media by means of glass micromodels. Geology 29, 867–870.
Waite, W.F., Santamarina, J.C., Cortes, D.D., Dugan, B., Espinoza, D.N., Germaine, J., Jang, J., Jung, J.W., Kneafsey, T.J., Shin, H., 2009. Physical properties of hydrate-bearing sediments. Rev. Geophys. 47.
Wang, J.-Q., Zhao, J.-F., Yang, M.-J., Li, Y.-H., Liu, W.-G., Song, Y.-C., 2015. Permeability of laboratory-formed porous media containing methane hydrate: observations using X-ray computed tomography and simulations with pore network models. Fuel 145, 170–179.
Wang, J., Zhang, L., Zhao, J., Ai, L., Yang, L., 2018. Variations in permeability along with interfacial tension in hydrate-bearing porous media. J. Nat. Gas Sci. Eng. 51, 141–146.
Wang, J., Zhao, J., Zhang, Y., Wang, D., Li, Y., Song, Y., 2016. Analysis of the effect of particle size on permeability in hydrate-bearing porous media using pore network models combined with CT. Fuel 163, 34–40.
Wang, J., Zhao, J., Zhang, Y., Wang, D., Li, Y., Song, Y., 2015. Analysis of the influence of wettability on permeability in hydrate-bearing porous media using pore network models combined with computed tomography. J. Nat. Gas Sci. Eng. 26, 1372–1379.
Wang, X.-H., Sun, Y.-F., Wang, Y.-F., Li, N., Sun, C.-Y., Chen, G.-J., Liu, B., Yang, L.-Y., 2017. Gas production from hydrates by CH4-CO2/H2 replacement. Appl. Energy 188, 305–314.
Wu, Z., Li, Y., Sun, X., Li, M., Jia, R., 2018. Experimental study on the gas phase permeability of montmorillonite sediments in the presence of hydrates. Mar. Pet. Geol. 91, 373–380.
Yang, J., Hassanpouryouzband, A., Tohidi, B., Chuvilin, E., Bukhanov, B., Istomin, V., Cheremisin, A., 2019. Gas Hydrates in Permafrost: Distinctive Effect of Gas Hydrates and Ice on the Geomechanical Properties of Simulated Hydrate-Bearing Permafrost Sediments. J. Geophys. Res. Solid Earth.
Yang, J., Okwananke, A., Tohidi, B., Chuvilin, E., Maerle, K., Istomin, V., Bukhanov, B., Cheremisin, A., 2017. Flue gas injection into gas hydrate reservoirs for methane recovery and carbon dioxide sequestration. Energy Convers. Manag. 136, 431–438.
Yang, J., Tohidi, B., Chapoy, A., 2008. Impact of sedimentary mineralogy on the geophysical and geomechanical properties of hydrate-bearing sediments, in: Sixth International Conference on Gas Hydrates, Sponsor, Vancouver, BC, Canada. pp. 6–10.
Zdravkov, B.D., Čermák, J.J., Šefara, M., Janků, J., 2007. Pore classification in the characterization of porous materials: A perspective. Cent. Eur. J. Chem. 5, 385–395.

Highlights

- Gas permeability of the sediments was measured under varying differential pressure.
- Effect of sediment mineralogy was investigated on gas permeability.
- Pore scale habits of hydrates was observed to control the gas permeability.
- Hydrate-forced heave was observed to be influential for sand-clay sediments.
- Capillary breakthrough and gas slippage could dominate gas permeability behavior.